DOI 10.5162/sensor2017/D6.2

Characterisation of a 5 MN·m Torque Transducer by Combining Traditional Calibration and Finite Element Method Simulations

P. Weidinger[1], Ch. Schlegel[1], G. Foyer[1], and R.Kumme[1]
[1] Physikalisch-Technische Bundesanstalt, Bundesallee 100, Braunschweig, Germany, Paula.Weidinger@ptb.de

Abstract:
Precise torque measurement in nacelle test benches increases the demand for an expansion of the torque measurement range up to several MN·m and a torque transfer standard. To this end, a 5 MN·m torque transducer was acquired. However, a traceable torque calibration is only possible up to 1.1 MN·m so far. This calibration is presented and discussed in this paper. In order to fully characterise the 5 MN·m torque transfer standard, a finite element analysis of the calibration setup is performed and validated using the gathered measurement data. Moreover, the Young's Modulus of the deformation body was determined using a force standard machine and a laser interferometer to acquire the longitudinal displacement of the deformation body due to compression. An estimation of the measurement signal over the entire measurement is given considering the partial range calibration results and the influences on strain gauge based measurements.

Key words: torque calibration in the MN·m range, torque transfer standard, strain gauge simulation, torque range extension

Introduction

Minimising downtimes and maximising service intervals of wind turbines can be achieved by nacelle testing as shown in Fig. 1. Furthermore, the efficiency of wind power plants can be determined reliably by measuring the input and output power in nacelle test benches as depicted in Fig. 1. Whilst the output power is measured as electrical output of the nacelle, the input power is quantified as mechanical power by recording the torque *M* at the nacelle's rotor hub.

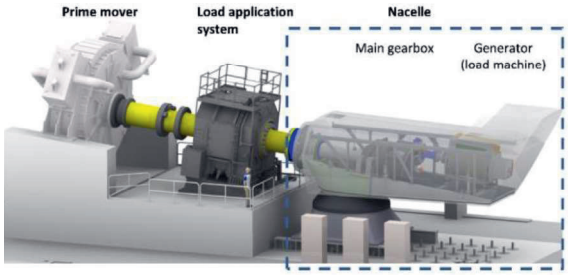

Fig. 1 Nacelle test bench at Aachen University including a Prime Mover, a Load Application System to simulate wind loads, and the nacelle under test (Source: CWD Aachen).

Modern wind turbines, having scaled up to multi-megawatt power ratings, give rise to increasing torques up to several MN·m at the rotor hub. In order to calibrate torque measurements in this high range on nacelle test benches, appropriate torque transfer standards (TTSs) are required. For this purpose, the German National Metrology Institute – Physikalisch-Technische Bundesanstalt (PTB) – acquired a 5 MN·m TTS using strain gauges (SGs) to convert torque into an electrical signal [1]. Even though the world's largest torque standard machine (TSM) to calibrate torque transducers is located at the PTB, the new 5 MN·m TTS can only be calibrated in a partial range up to 1.1 MN·m [2]. To achieve a full range characterisation of the 5 MN·m TTS, the partial range calibration and the usage of an adjusted finite element analysis (FEA) model are combined.

Torque Calibration up to 1.1 MN·m

Realising torque in the MN·m range can be realised by an active actuator-system and a force-lever measurement system. Since 2004, calibrations up to 1.1 MN·m based on this principle can be performed. Due to specially designed strain controlled elastic hinges, the TSM's uncertainty amounts to $8 \cdot 10^{-4}$ (k = 2).

As shown in Fig 2, the TSM's measuring axis *z* is vertical. At the bottom, the drive unit consisting of a double-sided lever arm, arranged in a free-floating matter, and two servo-electric spindles to apply the torque are

installed. By operating the main drives in the same plane and parallel, parasitic bending moments M_{z1} and M_{z2} (cf. Fig 9) can be minimised. A gear reduction at the spindles ensures a more precise triggering. In order to avoid hyper statics, all points of application are designed as cardan joints. The measuring unit is located on top of the measuring axis: the initiated moment M_z is split into a pair of nearly equal forces by a second double-sided lever arm which are measured by force transducers. For providing an alternative measuring system within the TSM, an additional TTS is installed above the lower lever.

Parasitic forces F_{x1} and F_{x2} in direction of the lever arm are to be reduced to a minimum by a re-adjustment of the horizontal lever arm position using a third, auxiliary drive. [2]

$$F_{x1} + F_{x2} \xrightarrow{!} \min \qquad (1)$$

Moreover, specially designed strain controlled hinges monitor the bending moments at both force-transducer-lever-junctions: M_{z1} and M_{z2}. While the parasitic forces can be neglected due to position optimisation of the measuring axis, the recorded bending moments are taken into account for the calculation of the applied torque M_z:

$$M_z = (F_1 \cdot r_1 + F_2 \cdot r_2) + M_{z1} + M_{z2} \qquad (2)$$

where r_1 and r_2 are the length of the lever from the force transducer to the rotation axis and, therefore, equal.

Fig 2 PTB's 1.1 MN·m torque standard machine (TSM) with a vertical measuring axis z.

The upper lever arm is carried by the machine frame to avoid additional mass on the transducer to be calibrated. Additionally, a vertically oriented servo-electric engine re-adjusts the lower lever arm in height after bolting all components to release the TTS from any axial tension or compression. This alignment is observed by the bending hinges and the appearing bending moments.

A well-established calibration standard for static torque calibration is the DIN 51309 [3] given by the German Institute of Standardisation. Acc. to this standard, the torque is applied clockwise and anti-clockwise separately; ideally without any bending moments and parasitic forces. Moreover, the torque is applied stepwise, and in different mounting positions. Based on the re-alignment of the measuring axis in the described TSM before starting the next measuring series, the transducer to be calibrated does not have to be rotated. However, the measuring series are treated as different mounting positions for the calibration evaluation acc. to DIN 51309.

Partial Range Characterisation of the 5 MN·m TTS

The new TTS is a hollow shaft type torque transducer with flange interfaces and a nominal capacity of $M_{z,TTS}$ = 5 MN·m. Furthermore, the TTS is equipped with additional measuring bridges for gauging the longitudinal force F_z with a limit of 30 MN, lateral forces $F_{x,TTS}$ and $F_{y,TTS}$ up to 8 MN and bending moments $M_{x,TTS}$ and $M_{y,TTS}$ of 3 MN·m.

Tab. 1 Relative measurement uncertainty interval (k = 2) considering clockwise and anti-clockwise torque separately for case II of DIN 51309 where the calibration results are taken from the increasing and decreasing series, averaged over the so called mounting positions and linearly fitted.

Torque in kN·m	Rel. uncertainty interval (k = 2) in %	
	Clockwise	Anti-clockwise
± 0	-	-
± 100	0.152	0.136
± 200	0.110	0.102
± 300	0.109	0.102
± 400	0.111	0.102
± 600	0.097	0.094
± 800	0.088	0.090
± 1000	0.084	0.083
± 1100	0.087	0.081

Owing to the lack of large TSMs, a calibration over the entire measuring range of the 5 MN·m TTS is not possible so far. Hence, the TTS is only calibrated up to 1.1 MN·m which equates to 22 % of the possible measuring range. This calibration was performed acc. to DIN 51309. As the TTS is supposed to be employed for measuring increasing as well as decreasing torque, the calibration result is calculated from the mean of the tared displayed values including the increasing and the decreasing series and averaged over the so called

mounting positions [3]. The relative uncertainty intervals separately for clockwise and anti-clockwise load and for the aforementioned case of application are listed in Tab. 1.
While, theoretically, the relation between the applied torque and the output signal is linear within the linear-elastic range, in reality, small nonlinearities appear even within this range. For visualisation reasons, the absolute linearity deviation d_{lin} is plotted against the applied torque. The linearity deviation for each torque step i is calculated by subtracting a linear regression curve with a slope m_{linear} from the tared signal output of each step $S_{meas}(i)$:

$$d_{lin}(i) = S_{meas}(i) - (m_{linear} \cdot M(i)) \qquad (3)$$

with M being the actual applied torque.

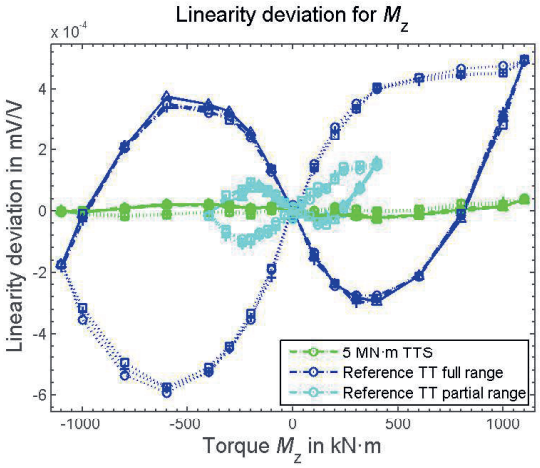

Fig. 3 Absolute linearity deviation from the best fit of the particular measurement range and separately for the 5 MN·m TTS and the reference transducer.

The absolute linearity deviation of the 5 MN·m (green) TTS is plotted in Fig. 3 together with d_{lin} of a well-known reference transducer (blue), which is part of the 1.1 MN·m TSM for monitoring reasons. The cyan curve in Fig. 3 shows that d_{lin} significantly depends on the measurement range and increases with the extension of the measurement range; here it is a partial measurement range up to 0.4 MN·m. The linearity of the 5 MN·m TTS is relatively small for the small measurement range of 22 %.

The difference between the calibration result of a calibration acc. to DIN 51309 and the associated value of the respective calculated regression curve step is indicated as the so called interpolation deviation. In this context, the regression curves can be determined using 1st or 3rd degree fitting functions. More and detailed information can be taken from DIN 51309 [3]. Generally, as it can be seen in Fig. 4, the interpolation deviations are within 0.07 % which is comparatively good and the cubic fitting function exhibits the smallest deviations. The first load step for both clockwise and anti-clockwise load always differs drastically.

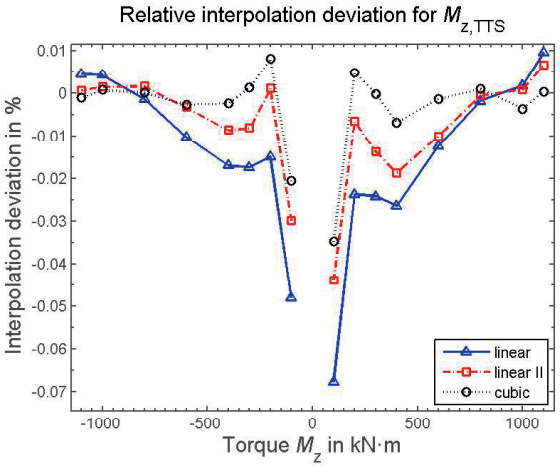

Fig. 4 Interpolation deviation for the $M_{z,TTS}$ bridge of the 5 MN·m TTS within the calibrated range of ± 1.1 MN·m relative to the actual value.

Determination of the Young's Modulus

For simulating the 5 MN·m TTS and, thereby, characterising it above 1.1 MN·m, which cannot be done in reality so far, the Young's Modulus of the deformation body is crucial. To determine this specific material parameter, the Young's Modulus, the deformation of the hollow shaft of the TTS due to compression is analysed as shown in Fig. 5.

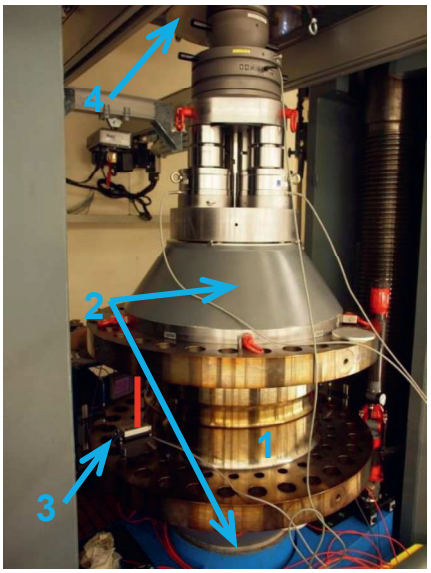

Fig. 5 5 MN·m TTS (1) in PTB's 16.5 MN FSM. Assembled with two load application plates (2) and two laser interferometer heads (3) on the y-axis tracking the deformation along the z-axis. The axial force is applied via the 16.5 MN machine's stamp (4) and the flux of force is closed by leading it back into the machine frame.

PTB's 16.5 MN force standard machine (FSM) [4] was deployed to apply axial compression to

the 5 MN·m TTS. To this end, the TTS was put between two load application plates because the compression stamp of the FSM was not big enough to transmit the compression into the transducer. Whilst applying defined compression to the TTS, the relative deformation of the hollow shaft was recorded by a two-channel homodyne quadrature HeNe laser interferometer [5]. The two laser heads were placed symmetrically and as close as possible to the hollow shaft. The application of compression took place in defined and very precise steps up to 4 MN to make sure the transducer does not get damaged.

Based on the relative length variation recorded by the laser interferometer heads, the Young's Modulus was determined by calculating the stress σ and the strain ε at the necking where the SGs are glued to. Fig. 6 visualises the calculated Young's Modulus for both laser heads separately and for the averaged signal plotted against the applied force steps. As can be seen in Fig. 6, the Young's Modulus is not constant over the applied force in the beginning but converges to approx. 195 GPa. These calculated values for the Young's Modulus were used for the FEA. While the rel. measurement uncertainties of both the 16.5 MN FSM with $1 \cdot 10^{-4}$ and the laser interferometer $< 1.5 \cdot 10^{-7}$ are comparably small, the geometry of the deformed part of the hollow shaft and the positions of the laser heads have a great influence on the determination of the Young's Modulus. Based on this, the uncertainty of the Young's Modulus is estimated with about 2.5 %. Furthermore, the Poisson's ratio cannot be determined based on this setup owing to the missing monitoring of the radial deformation of the hollow shaft in general and the necking in particular.

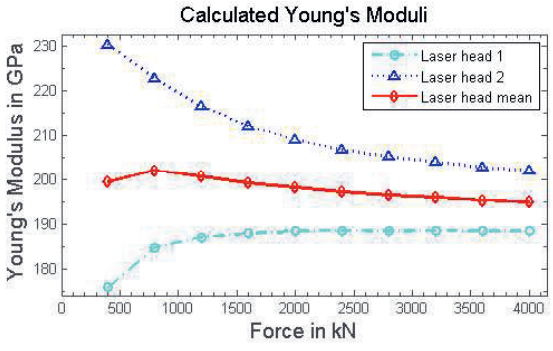

Fig. 6 Young's Modulus calculated by the applied force, the alteration in length and the profile of the transducer's hollow shaft.

Simulation of the Calibration Procedure

To achieve a realistic representation of the calibration procedure and, thereby, expand the characterisation of the TTS up to its full measurement range of 5 MN·m, the boundary conditions of the assembly are of great importance. The setup of the calibration axis of the 1.1 MN·m TSM was already described before. Since the reaction loads are only known for the measuring-lever side (I), the FEA is set up like the real TSM in reverse: the actuator-lever is fixed using remote displacement and specifying the degrees of freedom. At both sides, the actuator-lever is gimballed (II) which means the displacements in *x*- and *y*-direction as well as the rotation around the *x*-axis are locked (see Fig. 7). To avoid a movement of the calibration axis in *z*-direction, the remote displacement in the middle of the actuator-lever is locked in this direction (III). Furthermore, a remote displacement locked in *z*-direction holds the measuring-lever (IV) and relieves the TTS to be calibrated of any tension coming from the upper lever arm. All recorded acting forces and bending moments at the measurement-lever are induced at the coupling points between the force transducers and the measuring-lever (I).

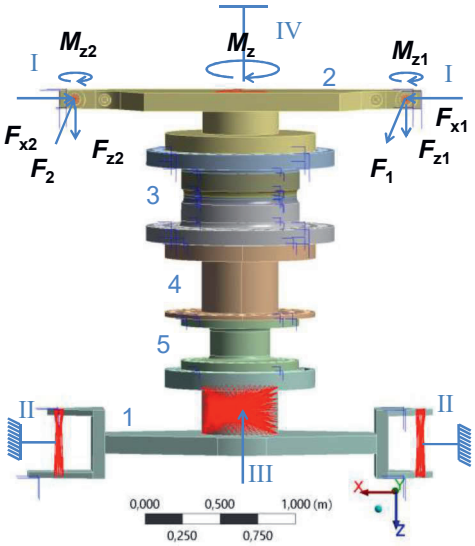

Fig. 7 Embedding of the actuator-lever (1) of the calibration setup and application of forces and bending moments at the coupling points between the force transducers and the measurement-lever (2). The applied torque M_z propagates from (2) through the TTS (3), the adaptor (4), and the reference transducer (5) back into (1).

The material parameters used for the TTS are based on the investigations aforementioned. Hence, the Young's Modulus for the TTS amounts to 195 GPa and the Poisson's ratio is assumed to be 0.3. For all other components of the calibration setup, the standard parameters for construction steel are deployed. The simulation was performed using the mechanical tool of the commercial software Ansys 17.2 for the increasing load steps as listed in Tab. 1 for clockwise torque.

Before the SGs can be modelled, some background information is of great importance: modern foil SGs (cf. Fig. 8) consist of an electrically insulating backing foil carrying the strain sensitive conductive lines (3) applied in a meandering pattern to enlarge the sensitive area, and a protecting cover panel. To shield the SG, not only against mechanical influences but also temperature, chemical influences, and especially humidity, the grid is hermetically sealed by a glue layer. The operating principle of SGs is given in Fig. 8: the deformation body is deformed by an applied load whereas, consequently, a strain ε_{DB} is generated. The strain ε_{BF} is transferred into the conductive lines via the adhesive layer and the backing foil. By straining this current-carrying conductor and thereby varying it in length and, thus, in profile, the electric resistance R of the grid changes: $\Delta R/R$.

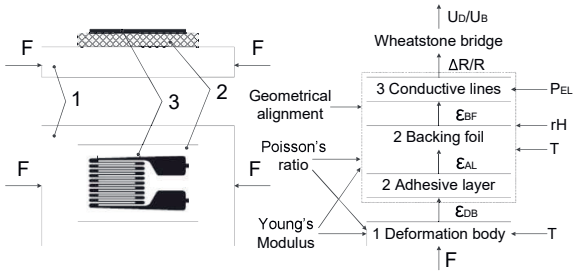

Fig. 8 Strain gauge (SG) consisting of an adhesive layer and a backing foil (2) and the conductive lines (3) glued to a deformation body (1).

For the 5 MN·m TTS several SGs are interconnected in a Wheatstone full-bridge configuration, so a torque dependent voltage alteration can be measured in mV/V:

$$\frac{U_D}{U_B} = \frac{k}{4} \cdot \left(\varepsilon_{SG1} - \varepsilon_{SG2} + \varepsilon_{SG3} - \varepsilon_{SG4} \right) \quad (4)$$

where U_D and U_B are the bridge output voltage and the bridge supply voltage, respectively. The correlation between the relative resistance alteration and the strain ε_{SG} is called gauge factor k. This also describes the sensitivity of the SG. The gauge factor for the employed SGs is $k = 2.05627$ with an uncertainty of 0.7 % given by the manufacturer. The calculated strain at the necking of the TTS based on the measurement signal and the applied torque of $M = 1.1$ MN·m is approx. $\varepsilon_{SG} = 138.88$ mm/m. The approximation of the Wheatstone bridge has its maximum of sensitivity for a symmetric setup, where all relative resistance alterations are equal, at 1/4 which is the reason for the factor 1/4 in (4). As the exact geometry of the utilised SGs is not known, the backing is assumed to be 13x13 mm² carrying four grids of 4 mm length and 3.5 mm width with an angle of 90° relative to each other. For the simulation, the SGs are modelled as Ansys shell element, SHELL181, with a thickness of 0.025 mm and a zero-stiffness.

Theoretically, the relation between the applied torque and the measurement signal is linear within the linear-elastic range of all components. From long calibration experience it is established that small nonlinearities appear even within the linear-elastic range. This was proven by the aforementioned calibration results of both the reference torque transducer and the 5 MN·m TTS. The nonlinearities can be evoked by the strain transmission through the different adhesive layers and the plastic backing foil of the SG due to their viscoelastic behaviour. In addition, the material characteristics of the deformation body are not completely linear as well, as shown by the compression measurement results (see Fig. 6). And also, a poor bonding quality can induce nonlinearities. Since the nonlinearities for the partial measurement range of 22 % of the 5 MN·m TTS are comparably small, this effect is not incorporated in the simulation. In principle, a SG calculates the arithmetic mean of the strain in place below the conductive lines.

$$\varepsilon_{FE,SG} = \frac{1}{A_{SG}} \cdot \int_{A_{SG}} \varepsilon_{FE} \, dA_{SG} \quad (5)$$

To describe this approach, the SG's grid is meshed in one as can be seen in Fig 9. Hereby, the single element A_{SG} for the grid represents the averaging of the strain $\varepsilon_{FE,SG}$ below it and simplifies the evaluation of the simulation results and the consequent calculation of the interconnected output signal. According to [6], the strain transmission from the deformation body into the measuring grid can vary from 96 % up to nearly 100 %. In the simulation, the contact between the deformation body and the SGs is represented by a contact region of the type bonded. To make sure, the penetration of the contact does not lead to a change of the very same thing, the pure penalty algorithm is used. Also very important for good simulation results is the meshing of the transducer in general and the necking including the inlet zones in particular. This was done using the Sweep-Method and Submodelling of the above outlined part of the TTS.

The model of the calibration setup is validated by the calibration data gathered up to 1.1 MN·m. While the simulation result highly depends on the meshing, the measurements using SGs are contingent on several influence quantities. All possible influences were analysed and categorised. As a result, merely

the significant influences on the measurement of mechanical strain are listed in Tab. 2. Variations due to temperature alterations are not taken into consideration owing to the stable ambient conditions that prevailed during the calibration procedure. Furthermore, misalignment and eccentricity errors of the calibration axis setup are not further analysed but taken from [7] and [8] for other machines.

Tab. 2 Influence quantities and their estimate on the measurement using SGs.

Influence quantity	Estimate
Uncertainty of Young's Modulus of def. body and SGs	5 %
Bending of the SG	~ 0.03 %
Alignment of the SG	-1 %
Gauge factor uncertainty	0.7 %
Linearity (within linear-elastic range)	0.1 %
Self-heating of the SG by the bridge supply voltage	negligible
Uncertainty of the employed amplifier ML38 (HBM)	0.0025 %
Misalignment error of calibration axis components	0.01 %
Eccentricity error of calibration axis components	0.005 %

In Fig 9, the principal strain at the necking of the 5 MN·m TTS for a mesh with eight elements over the necking height and an edge length of 2.5 mm is depicted. The modelled SGs show nearly the same normal elastic strain in deformation direction of each grid based on the elemental triad of the respective grid. For this not very accurate meshing relative to the size of the SGs, the signal output calculated by (4) deviates from the measured signal by approx. 17.5 %. In order to characterise the TTS above the measurable range, a linear calibration factor can be used due to the negligible nonlinearities as described before.

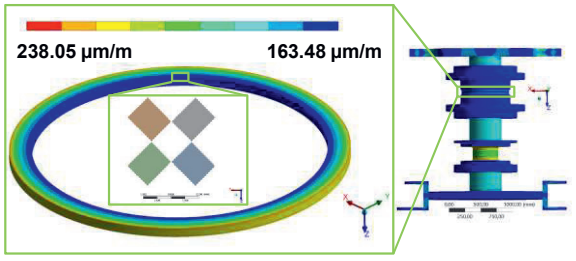

Fig 9 The FEA results for the calibration axis of the 1.1 MN·m TSM including the 5 MN·m TTS and principal strain at the necking of the 5 MN·m TTS. The SGs are modelled as Shell elements.

Conclusion and Future Work

A new 5 MN·m TTS was calibrated in a partial range of 22 % which corresponds to 1.1 MN·m. The determined maximum nonlinearities of $\pm 1.1 \cdot 10^{-4}$ mV/V are negligibly small by comparison and the relative uncertainty (k = 2) is < 0.15 %. Additionally, these calibration results were used to validate a FEA-model including not only the 5 MN·m TTS but also the overall design of the employed 1.1 MN·m TSM's calibration setup. Based on the FEA-model, the 5 MN·m TTS can be characterised exceeding the actual calibrateable range using a calibration factor.

Further investigation about the influences of eccentricity and misalignment of the calibration setup could be done in parameter studies using FEA. Moreover, an approach to rate an uncertainty budget for the extended measurement range is to be developed. To this end, the nonlinear behaviour of a variety of torque transducers is to be measured and analysed in different measurement ranges in the future.

Acknowledgements

The authors would like to acknowledge the funding of the Joint Research Project "14IND14 MN·m Torque - Torque measurement in the MN·m range". This project has received funding from the EMPIR programme co-financed by the European Union's Horizon 2020 research and innovation programme and EMPIR Participating States.

The lead author gratefully acknowledges support by the Braunschweig International Graduate School of Metrology B-IGSM.

References

[1] R. Schicker, G. Wegener, Measuring Torque Correctly, *Bentrup Druckdienste KG, Bielefeld*, (2002)

[2] D. Peschel, D. Mauersberger, D. Schwind, U. Kolwinski, The new 1.1MN·m torque standard machine of the PTB Braunschweig/ Germany, *19th IMEKO TC3, Cairo, Egypt*, (2005)

[3] DIN Deutsches Institut für Normung e.V., Material testing machines - Calibration of static torque measuring devices, DIN 51309:2013-09, Technical *Commitee Drehmoment of Deutscher Kalibrierdienst*, (2013)

[4] R. Kumme, F. Koehler, PTB's 16.5 MN hydraulic amplification machine after modernization, *22nd intl. Conference of IMEKO TC3, Cape Town*, Vol. 22, (2014)

[5] D. Dontsov, Interferometric concept and product overview, (2014)

[6] M. Stockmann, Mikromechanische Analyse der Wirkungsmechanismen elektrischer Dehnungsmessstreifen, *Habilitationsschrift, Chemnitz,* (1999)

[7] A. Brüge, D. Peschel, D. Röske, The Influence of Misalignment on Torque Transducers, *16th IMEKO World Congress, Vienna, Austria,* (2000)

[8] A. Brüge, Influence of Eccentric Mounting on the Calibration of Torque Measuring Devices, *15th IMEKO TC3, Madrid, Spain*, pp. 255–259, (1996)